이학석사 학위논문

Low Temperature Scanning Tunneling Microscope with Improved Head Design and Its Application to The Study of $Bi_2Sr_2CaCu_2O_{8+x}$ Single Crystal

저온 주사 터널링 현미경을 위한 개선된 헤드 디자인과 이를 이용한 $Bi_2Sr_2CaCu_2O_{8+x}$단결정 연구

2017년 2월

서울대학교 대학원

물리천문학부

곽 정 수

Low Temperature Scanning Tunneling Microscope with Improved Head Design and Its Application to The Study of $Bi_2Sr_2CaCu_2O_{8+x}$ Single Crystal

저온 주사 터널링 현미경을 위한 개선된 헤드 디자인과 이를 이용한 $Bi_2Sr_2CaCu_2O_{8+x}$ 단결정 연구

지도교수 이 진 호

이 논문을 이학석사 학위논문으로 제출함

2017년 2월

서울대학교 대학원

물리천문학부

곽 정 수

곽정수의 이학석사 학위논문을 인준함

2016년 12월

위 원 장 박 윤 (인)

부위원장 이 진 호 (인)

위 원 김 창 영 (인)

Low Temperature Scanning Tunneling Microscope with Improved Head Design and Its Application to The Study of $Bi_2Sr_2CaCu_2O_{8+x}$ Single Crystal

Jeong-Soo Kwak

supervised by

Professor **Jinho Lee**

A Dissertation
Submitted to the Faculty of
Seoul National University
in Partial Fulfillment of
the Requirements for the Degree of
Master of Philosophy

December 2016

Department of Physics and Astronomy
Graduate School
Seoul National University

Abstract

Low Temperature Scanning Tunneling Microscopy (LT-STM) is a valuable tool not only in surface science but also, in condensed matter physics. Here, we present three improvements in Ultra Low Vibration (ULV) Lab and LT-STM design : tip treatment stage, sample cleaving stage and vibration isolation system. Improved tip treatment stage enables us to perform field emission for a tip treatment *in-situ* without exchanging samples, while our enhanced sample cleaving stage allows us to cleave samples at low temperature in vacuum without optical access by a simple pressing motion. Our newly designed vibration isolation system provides an efficient space usage while maintaining a vibration isolation capability. These improvements enhance the quality of spectroscopic imaging experiment which can last for many days and also provide an increased data yield. On the other hand, since Nanonis STM™ (Generic4) controller comes with basic default sets of functions while it lends an expendability in its functionality via Labview™, we added additional customized protocols for our experimental method of choice : Spectroscopic Imaging STM (SI-STM). In addition, since the library of analysis tools accumulated over decades for an outdated topometrix™ STM controller is vast and comprehensive, we choose to write a C++ protocol which can convert raw data form at from

Nanonis to a data form at which is compatable with already existing such analysis programs rather than creating entire analysis library from the scratch. Finally, we demonstrated SI-STM performances at 4K on highly overdoped $Bi_2Sr_2CaCu_2O_{8+x}$ using ULV Lab facility which is much more compact than conventional ULV Lab design.

In this thesis, I will describe such improvements in STM instrumentations as well as in softwares for STM controls and data analysis.

keywords : Sample Cleaving System, Tip Treatment Stage, Vibration Isolation, Nanonis Controller
Student Number : 2014-21356

Contents

List of Figures

List of Figures

Chapter 1
Introduction

1.1 Spectroscopy Using Scanning Tunneling Microscope

Since the invention of scanning tunneling microscope (STM) by Binnig and Rohrer[1-3] in 1982, it immediately became a powerful tool in condensed matter physics for exploring surface, electronic structure and bulk properties in atomic resolution. To achieve atomic resolution, it requires good tip condition, clean sample surface and vibration isolation system. In our homebuilt STM design, in order to maximize the stability of STM, we exclude the sample preparation chamber. Instead, we choose to cleave sample *in-situ* in high vacuum and cryogenic environment to achieve clean sample surface. Moreover, maintaining the tip apex as a radius of one atom requires tip treatment method. Here, we describe our STM design including improved STM head, sample cleaving stage and vibration isolation system. Improved STM head has *in-situ* tip treatment stage. The *in-situ* tip treatment stage helps to maintain non invasive experimental environment[4-6] at the same time it saves a lot of time compared to pre-existing tip treatment method. Sample cleaving stage allows us to cleave samples by simple pressing motion. It is much

more convenient and more importantly it reduces a risk of dropping samples while sample transfer. Our newly designed vibration isolation system provides efficient space usage with maintaining a vibration isolation ability. These extend the experiment lifetime and provide high quality of spectroscopic images. We demonstrated $Bi_2Sr_2CaCu_2O_{8+x}$ (BSCCO) cuprate[7,8,14] superconductor spectroscopic images and topograph.

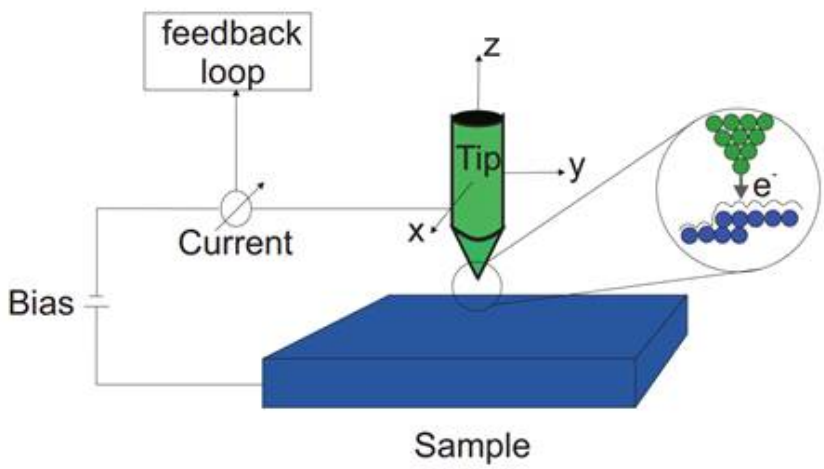

Figure 1.1 Schematic diagram of scanning tunneling microscope. Scanning tunneling microscope's probe is tip. The apex of the tip is ideally a radius of one atom. To maintain the set current, z piezo

Previous microscopes such as optical microscope and electron microscope are featured as long wavelength. It makes hard to see atomic scale. STM's operating mechanism is tunneling effect. This quantum mechanical property is revealed between sharp tip and sample. Figure 1.1 represents a schematic diagram of STM. A bias voltage is applied when a tip approaches to a sample until the tunneling current reaches a set current. Feedback circuit maintains

current by manipulating z-position. Because tunneling current between tip and sample should be only a function of distance, it is possible to produce a map of z-position. X and Y piezo control the position of measurement area. The collection of the data of z position at set current is topograph.

Another big feature of STM is spectroscopy. We can acquire $I-V$ curve by measuring the current with voltage sweeping. When $I-V$ curve is measured, feedback circuit must be turn off and the position of the tip must be kept. However, what we want to see is dI/dV curve. Because dI/dV curve is proportional to a local density of state (LDOS).[9]

$$\frac{dI}{dV} \approx \rho_S(E_F + eV)\rho_T(E_F) \tag{1}$$

is density of state of sample at energy E, is density of state of tip at energy E, is fermi energy and V is bias voltage between tip and sample. When a positive bias voltage is applied to sample, the fermi energy of the sample is lowered by eV respect to the tip. Electrons of the tip tunnel the potential barrier. dI/dV can be acquired from differentiating $I-V$ curve. But, for accuracy of data, we use lock-in technique. Lock-in gives small modulation to sample bias voltage. This is given as,

$$V = V_0 + V_{\mathrm{modulation}}\sin(\omega t) \tag{2}$$

Then the tunneling current is modulated and it can be expended by Taylor series.

$$I(V) = I(V_0) + \frac{dI}{dV} V_{modulation} \sin(\omega t) + \frac{1}{2} \frac{d^2 I}{dV^2} V_{modulation}^2 \sin^2(\omega t) + \ldots \quad (3)$$

By choosing first harmonics at lock-in amplifier, we can obtain the value, which is proportional to dI/dV. Like topograph, we can measure the dI/dV curve at various position and then we can get scanning tunneling spectroscopy (STS) map. From the STS map, we can see electronic structure, orbital degree of freedom, etc.

1.2. Nanonis STM Controller

Nanonis electronic control unit from SPECS is main control system of STM operation. It is composed to several units with different function. It includes RC4, PMD4, HVS4, HVA4 and SC4. RC4 is base unit which is connected to control computer by Ethernet cable. It also communicates other units. PMD4 is piezo motor driver. It is used when tip approaches to sample. It generates sawtooth like waveform which makes 'walker' walk. HVA4 is high voltage supplier and HSV4 is high voltage amplifier. SC4 is analog input output conversion unit. It has 8 inputs and outputs. It collects various signals and manipulates each signals.

Powerful feature of Nanonis control system is its software interface. Nanonis software interface is written in LABVIEW and it provides nanonis programming interface. By using this, we can operate various customizing experiments. All experiments and modules are operated by sequence of small behaviors. For example, bias spectroscopy is composed of 'get session path.vi', 'signal names

get.vi', 'bias spectroscopy channels set.vi', 'voltage get.vi', 'get timmings.vi', 'ctrl on off get.vi', etc. By using these parts, we can compose various experiments. Figure 1.2 shows example of Nanonis programming interface parts.

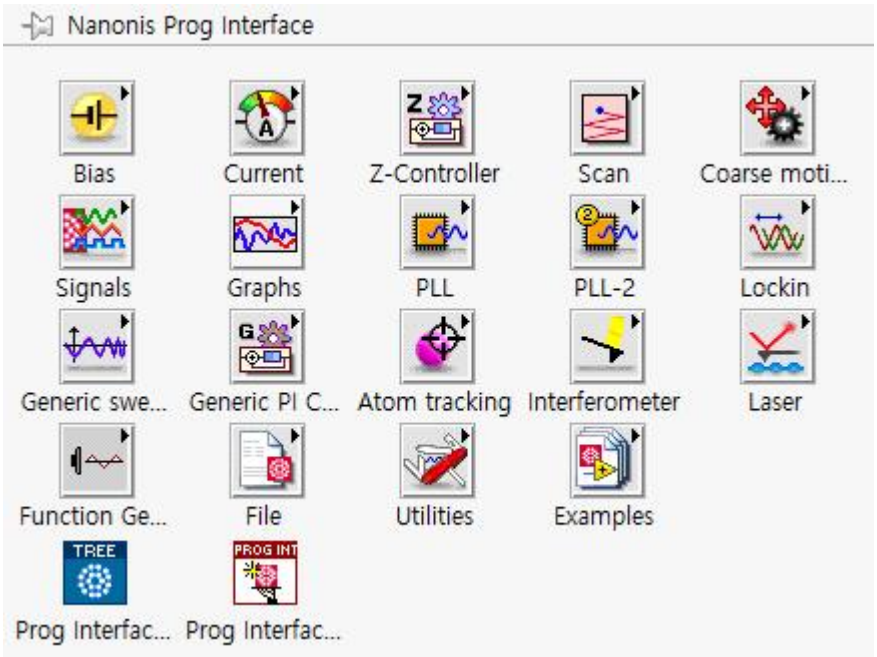

Figure 1.2 Example of Nanonis programming interface. It contains various parts and the parts are grouped by small modules.

Chapter 2
Software

2.1 Methodolgy of SI-STM

Bias spectroscopy is a basic component of Nanonis software. When we select interesting area and input grid number, it separates the area by given grid number then moves tip to first grid point. At the grid point, it holds the feedback to prevent any movement of the tip while sweeps bias voltage from given start bias to given end bias for acquisition of dI/dV curve. After bias sweep, tip moves to each grid points and repeats this procedure. This is simple bias spectroscopy experiment on grid. However, because tip is too close to sample, it is possible that tip collided with sample when it moves to other grid point. To prevent this problem, we modified bias spectroscopy by using Nanonis programming interface. The idea of modification is 'set different setpoints between spectroscopy phase and topograph phase'. Changing setpoint means changing tip-sample distance. Higher setpoint means closer to sample and lower setpoint means father to sample. By inserting 'Z-ctrl setpoint set.vi', we can lower setpoint (retract tip from sample) at topograph phase. For reducing fluctuation occurred by modification of setpoint, we insert setting time (waiting time) right after modification of setpoint. Also,

setpoint is changed gradually for reduce the fluctuation occurred by modification of setpoint. At spectroscopy phase, we can increase setpoint by use of 'Z-ctrl setpoint set.vi'. As a result, tip moves to sample closer than topograph phase. The concept of new spectroscopy experiment design is represented in figure 2.1. The blue line of figure 2.1 is trajectory of the tip. Conventional experiment design maintains tip-sample distance while measuring spectroscopy, but newly designed spectroscopy experiment changes the tip-sample distance according to the phase of experiment. When we measure the topograph, the junction resistance is 10 GOhm. When we measure the spectroscopy the junction resistance is 1 GOhm. Higher junction resistance means lower setpoint. Change of setpoint is implemented by 'for-loop' of Labview. The code for increase of setpoint is illustrated in figure 2.2. 'Z-ctrl setpoint get.vi' gets the currently given setpoint. There are three lines which are started from 'Z-ctrl setpoint get.vi'. The top line establishes connection between code and Nanonis controller. The bottom line returns error out. The given setpoint follows middle line. The outer most structure of the code is for-loop. It repeats same procedure inside the structure. Each  icon means initial value of the for-loop. The setpoint achieved by 'Z-ctrl setpoint get.vi' is saved at  as a initial value of the for-loop. It follows the connected line from left to right. This value increases by '1p' at the '+' icon. The increased value follows the connected line. At the circle on the line, the line divided into two. The increased value follows both of the line. At the end of the one line, the increased value is given to 'Z-ctrl setpoint set.vi'. It sets the setpoint as the increased value. For example, if the start value is 10p, it increased as 11p at the '+' icon and than it is given to 'Z-ctrl setpoint set.vi'. As a result, 'Z-ctrl setpoint set.vi' changes setpoint from 10p to 11p. At

the end of the other line, the increased value is saved at icon. This icon changes the initial value of the for-loop. For example, let's assume the initial value is 10p. After icon, the for-loop is restarted from icon. However, the saved value in the icon is no longer 10p. It is 11p. This procedure is repeated inside the for-loop. As a result, the setpoint increase 1p by 1p until given iteration is satisfied. icon sets the iteration of the for-loop and 'milliseconds to wait' sets waiting time at the end of each increase of setpoint.

Like setpoint, bias voltage is changed between moving phase and spectroscopy phase. Changing bias voltage is done by same mechanism with changing setpoint. At the spectroscopy phase, because the tip-sample distance is too close, all other manipulation must be done at topograph phase for the safety of the tip. Change of distance between tip and sample must be done carefully. So, change of the setpoint and bias voltage must be done after change of integration gain. Integration gain controls the speed of tip. Before change of the setpoint and bias voltage, we must lower integration gain for slow down the speed of the tip. It makes safe approach to sample.

The block diagrams of conventional spectroscopy experiment and newly designed spectroscopy experiment are shown in figure 2.3. Conventional spectroscopy experiment only consist of three steps. Newly designed spectroscopy experiment contains several steps to protect tip from damages. The source Labview flat sequence code for new spectroscopy experiment is attached at APPENDIX.

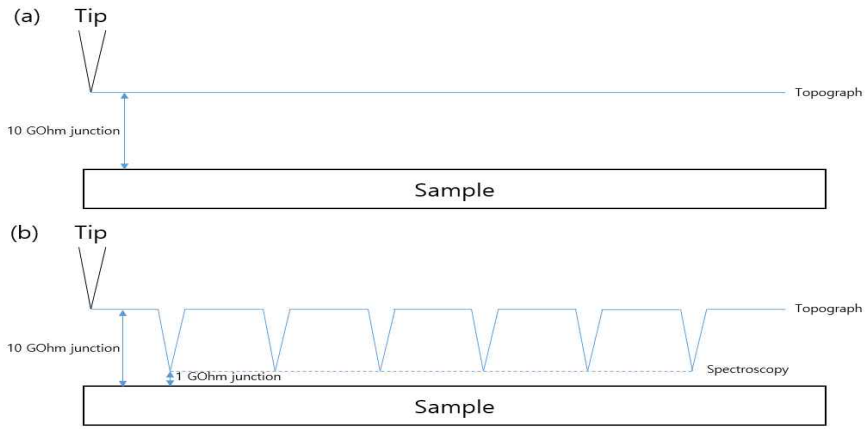

Figure 2.1 Schematic diagram of new spectroscopy experiment. (a) is conventional experiment design. It maintains the tip-sample distance. The blue line represents the trajectory of the tip. (b) is new spectroscopy experiment design. The junction resistance is changed from 10 GOhm to 1 GOhm as we measure the spectroscopy.

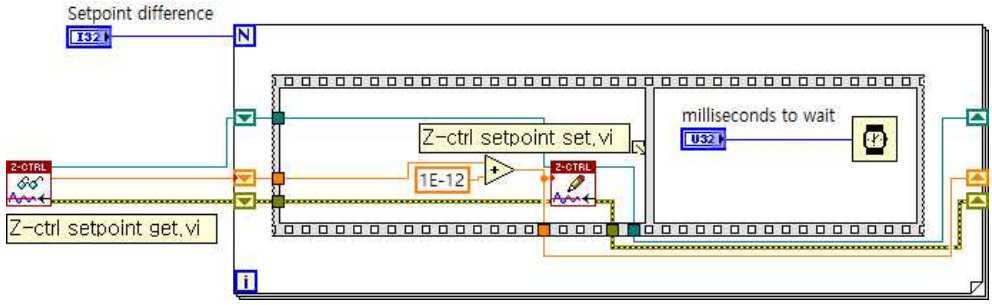

Figure 2.2 Labview code for change setpoint. 'Z-ctrl setpoint get.vi' returns the Z-controller setpoint. 'Z-ctrl setpoint set.vi' sets the Z-controller setpoint. Setpoint increase by 1pA per loop. After increase of setpoint, we can set waiting time for stabilization.

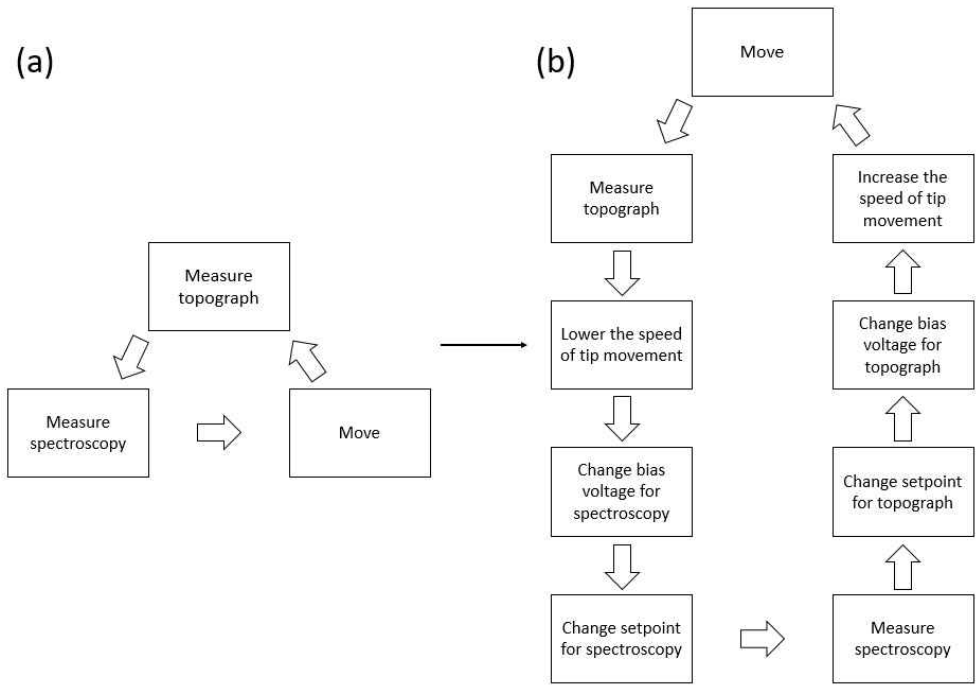

Figure 2.3 Block diagram of new spectroscopy measuring method. (a) is block diagram of conventional spectroscopy experiment. (b) is newly designed spectroscopy experiment. It measures spectroscopy and topograph simultaneously with safe condition.

2.2. Lock-In Technique

Nanonis controller basically offers internal lock-in module. It also offers option that turn on internal lock-in during the bias spectroscopy. However, because the performance of the Standford Research SR830 DSP lock-in amplifier (SR830) is better than the internal lock-in, we use SR830 for acquisition of dI/dV. To do this, SR830 should communicate with Nanonis. To communicate with Nanonis, A/I BNC plug of SR830 is connected to AI1 BNC plug of

Nanonis SC4 and sine out BNC plug of SR830 is connected to AI4 BNC plug of Nanonis SC4. Also, CH1 OUPUT BNC plug of SR830 is connected to AO4 BNC plug of Nanonis SC4. Between Lock-in and BNC cable, there are 10kHz low-pass-filters to cut off electrical noise.

We can change Nanonis bias output mode such as 'User output', 'Monitor' and 'Calculate signal'. 'User output' gives bias as written value in the software. 'Monitor' gives bias same as selected channel such as AO1, AO2, etc. 'Calculate signal' mode gives bias as calculated signal such as 'input 1 + input 2', 'input3 + output4', etc.

To use the external lock-in, following conditions must be satisfied. 1. The modulation of external lock-in is given to sample bias only during spectroscopy. 2. The modulation of internal lock-in do not interact with sample bias. Through AI4, the modulation of the SR830 is always given to Nanonis SC4. However, because of the condition 1, we must give modulation of SR830 to sample only during spectroscopy. To do this, we use the option that turn on internal lock-in during the bias spectroscopy. These are implemented by simple Labview programming. We can see it from figure 2.4. 'OpenAppRef.vi' establishes connection between code and controller. Outer most structrue is while-loop. It repeats inside process until someone clicks the stop button. 'Lockin on_off get.vi' returns 'true' or 'false' depend on the state of internal lock-in. If the internal lock-in is on, it returns true or it returns false. We can use modulation signal as output signal through 'Calculate signal' of output mode. By adding modulation signal of AI4 to sample bias, we can use external modulation of SR830. By using case structure of Labview, we can set output mode as 'Sample bias + external modulation' while 'lockin on_off get.vi' returns true. It means modulation of SR830 is given to

sample during internal lock-in is on. The fact that internal lock-in is on means spectroscopy is being measured. In short, SR830 gives modulation to sample only during spectroscopy. At the 'false' state, we can remove external modulation from sample bias by setting output mode as 'Monitor'. The structure which contains 'User ouput Mode set.vi' are case structure. It receives the boolean value of 'Lockin on_off get.vi'. The block diagram of lock-in control system is displayed at figure 2.5. 'Get Date/Time in seconds.vi' is used to calculate period of a single loop. In the internal lock-in module of Nanonis, there is option that choose channel which generates modulation. By selecting channel which is unrelated to sample bias, we can satisfy the second condition.

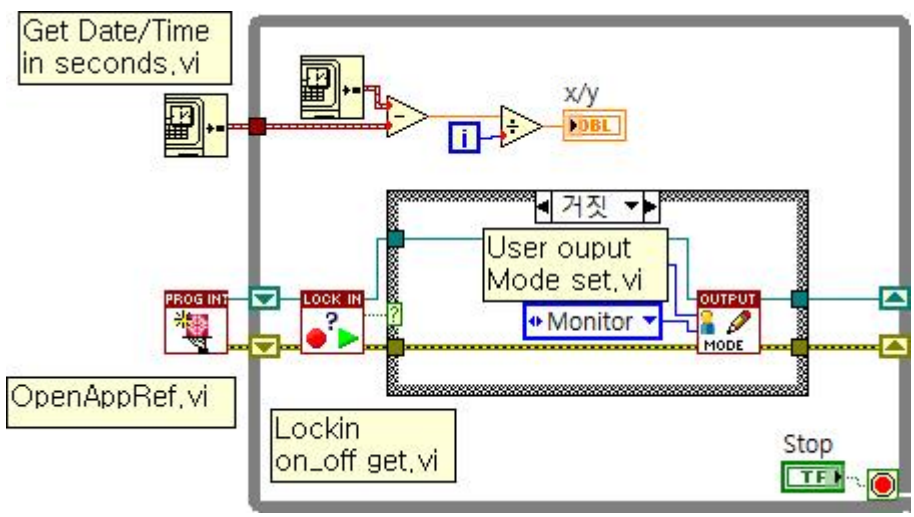

Figure 2.4 Labview code for lock-in control. 'OpenAppRef.vi' establishes connection with the nanonis control software. 'Lockin on_off get.vi' returns if the internal lock-in is running or not. 'User output Mode set.vi' sets bias module. If the case structure is true, it returns Calc.Signal. If the case structure is false, it returns monitor. 'Get Date/Time in secons.vi' is used to calculate period of a single

loop. The period of loop will be used to regulate setting time of bias spectroscopy. 'x/y' icon shows the value of period of the while loop. 'Stop' icon breaks the while loop.

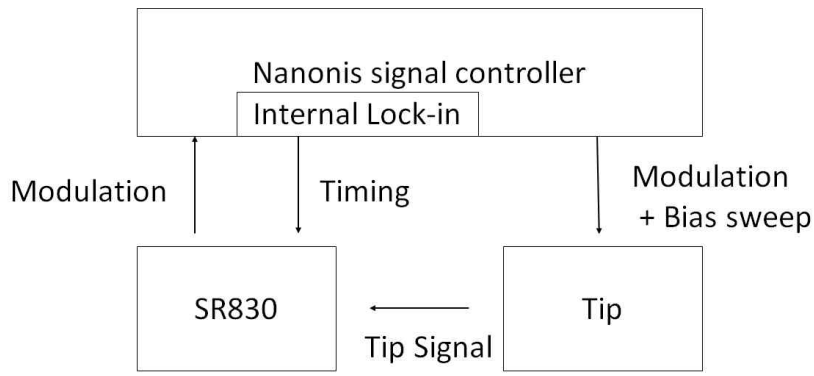

Figure 2.5 Block diagram of Lock-in control system. Internal lock-in is only used as trigger. External Lock-in (SR830) gives modulation when the trigger signal is given from internal lock-in. Tip signal is measured by SR830.

2.3. Data Conversion

Topographic image is saved as SXM file format in Nanonis. Z spectroscopy is saved as DAT file format and bias spectroscopy is saved as 3DS file format in Nanonis. DAT file format can be read simply by Microsoft Excel. SXM can be read WSXM. WSXM is a popular Windows application for data acquisition and processing in Scanning Probe Microscopy (SPM) and a wide range of microscopy or spectroscopy technique. There are many software to analyze DAT and SXM file format. However, there is no software to analyze 3DS file format. Our laboratory uses WAutility based software to analyze spectroscopy data as a 1FL file format. 1FL file format has data of spectroscopy map like 3DS. If we can convert 3DS to 1FL, we can

analyze spectroscopy data by using our analysis tool.

To convert 3DS to 1FL, we must know the data structure of 3DS and 1FL. Data structure of 3DS is explained in Nanonis manual. It consists of ASCII format header and binary data. The header consists of key-value pairs separated by an equal sign ('='). Some keys are mandatory, but arbitrary items can be added at will. An example of a key-value pair is (without the single quotes): 'Grid dim="24 x 24"'. The value is enclosed by double quotes if it contains spaces. Function '*void findequal (FILE *p)*' finds equal sign. Because the key values exist right after equal sign, finding equal sign is the most effective way to find key values of the header. The header is finalized by a line containing the text ':HEADER_END:' followed by the windows end of line characters CR/LF (carriage return/line feed; ASCII codes 0D and 0A). The following keys are defined (required) in version of the binary file format. Table of header is attached at table 2.1.

Table 2.1 Header of 3DS file format.[10]

Grid dim	Dimension of the grid in number of points. Format is 'Nx x Ny' with Nx = Number of points in x, Ny = Number of points in y.
Grid settings	Grid position and dimension in physical units (m). Format is 'Cx;Cy;W,H,A' with Cx = grid center x, Cy = grid center y, W = grid width, H = grid height, A = angle. Cx, Cy, W, H are in meters (m), A in degrees (deg).
Sweep Signal	Name of the sweeped parameter. This is a string, usually a signal name followed by its units in brackets. Example: 'Bias (V)'.
Fixed parameters	List of required parameters. These are stored at the beginning of each experiment. Usually the fixed parameters are 'Sweep Start' and 'Sweep End', i.e. the limits of the sweep signal.
Experiment parameters	Additional parameters stored for each experiment. These can contain the position where the experiment is taken ('X (m)', 'Y (m)', 'Z (m)') and other paramters. It's recommended to store at least the Z position as a parameter as this can be used to reconstruct the topography afterwards.
# Parameters (4 byte)	Total number of parameters stored with each experiment (= number of fixed parameters + number of experiment parameters). Each parameter is stored as a single precision floating point number using 4 bytes (big-endian).
Experiment size (bytes)	Size of experiment data in bytes. Each floating point number uses 4 bytes. When acquiring 1 channel forward and backward, 256 points, this will be 2 x 256 x 4 bytes = 2048 bytes.
Points	Number of acquired points in the experiment (e.g. bias spectroscopy).
Channels	Channels acquired in the experiment, separated by semicolons (';'). When acquiring data forward and backward 2 channels will be listed. Example: 'Current (A);Current [bwd] (A)'.
:HEADER_END:	End of header.

After the header, the binary data begin. All data is stored in 4 bytes big endian floats with the most significant bit (MSB) first. The experiments aren't separated. All data is written right after header continuously. Each experiment starts with the fixed parameters, followed by the experiment parameters and the experiment data (Channels one after the other). The size of the experiment data is defined in the header so it's easy to find a specific experiment. From the start of the binary data an experiment including the fixed and experiment parameters always takes (# Parameters) * 4 + (Experiment size) bytes.

Reading 3ds file format has some problem. Because header is changed when we select other signal channel, we fixed number of parameter to control size of header. Binary data are stored in big endian floats. However, Microsoft visual studio reads float by little endian, so we must convert every float from big endian to little endian. Memcpy (void * destination, const void * source, size_t num) is used to convert endian format. Function '*float Varread (FILE *p)*' performs endian conversion from big endian to little endian. It reads 4 bytes big endian float and than flips the sequence of bytes. Flipped sequence is saved by 'Memcpy'. After that, The function 'Varread' returns little endian float. Because data are saved as binary, we should use 'rb' when file open regardless of header format. After header, several information of data are saved such as position of X and Y, spectroscopy bias range and Z. However, there is no direct information about scan size, so we shold calculate the size of scan area. Function '*float distance (float a, float b, float c, float d)*' simply calculates the distance between two point and function '*float rounding (float a)*' refines scan size information to integer angstrom format. After these, spectroscopy data are saved such as current, Lock-in X

and Lock-in Y. These structure is repeated. So, we can read data by using 'for loop'. We can analyze 1FL structure by use of WAutility, data analysis software. Unlike 3DS, 1FL has very difficult header structure. However, this software can read 1FL file. It means we can found read 1FL file function from the source code of WAutility. From the function of WAutility, we found 1FL has very complex header structure. It consists of several classes and many unknown parameter. It takes long time to find what the parameter means. It can be solved by use of reference file. Many variables are fixed variables. We just change key variables at exact positions. The other issue of data conversion is data format. 3DS consists of 4 bytes floats but 1FL consists of 2bytes unsigned shorts. Function '*unsigned short dataconversion (float max, float min, float data)*' it main function of conversion. It converts 4 bytes float to 2 bytes unsinged short by use of maximum and minimum value of data. Nanonis SC4 handles voltage from -10V to 10V. It means 1FL has resolution 20(voltage difference)/65535(unsigned short range). It means data conversion from 3DS to 1FL makes data quality low. There are some solutions of this problem at section 4. Because the lock-in parameters are not contained at 3DS, we must insert lock-in parameters manually. The code of conversion 3DS file is attached at APPENDIX.

Chapter 3
Hardware

3.1 Sample Cleaving Stage

Cleaving is one of the methods to prepare an atomically flat surface. Since we heavily rely on cleaving in vacuum for sample surface preparation, sample cleaving stage is one of the most important parts in STM. There are two contingencies for the cleaving : 1. Easy to operate without optical access. 2. Minimizing mechanical frictions not to break vacuum environment. To meet these conditions, we designed the cryogenic sample cleaving stage which can be operated by single pushing motion. The details of sample cleaving stage are shown in figure 3.1 a, b, c. Its overall size is ~cm and it consists of body, press plate, cleaving basket and radiation blocker. Press plate and radiation blocker are made of Stainless steel 316 and the other parts of sample cleaver assembly are made of Oxygen free high conductivity copper (OFHC). To prevent oxidization after sample cleavage, sample cleaving stage needs to be installed inside the lower part of cryostat where the interior of cryostat is kept in ultra-high vacuum as well as at low temperature. Hence, sample cleaving stage is installed at the entrance of 4K stage of cryostat so that we can cleave samples at 4K.

Our sample transfer system has ability to exchange samples without warming up the system. Sample transfer is by top-loading and attached to sample stud that is fitted with the end of sample transfer rod.

Once sample is transferred to the entrance of 4K stage where the sample cleaving stage is located, it rests there about an hour to be cooled sufficiently. After cool down, sample stud is rotated and transferred to the top of the press plate (figure 3.1 b) through the key hole (figure 3.1 a). All cleaving procedure is depicted in figure 3.2. Note that we remove unnecessary parts and show all parts transparently in the figure 3.2 except cleaving rod and copper rod (figure 3.2 b, c, d) for a clarity. Red rod represents a cleaving rod attached to the sample and blue rod represents a hammering pin which knocks off the cleaving rod. One side of sample is attached to sample stud and another side of sample is attached to head of cleaving rod. To cleave the sample, one presses the sample transfer rod to let the sample stud press against the push plate. As sample stud presses the press plate, it forces the cleaving basket to rotate. (figure 3.2. C) Consequently, the hammering pin hits the cleaving rod and detach the cleaving rod from the sample and hence the sample gets cleaved. After the sample cleaving, the spring, which connects body and cleaving basket, brings cleaving basket back to the original position to clear the path for the sample transfer rod to place the sample stud with the cleaved sample inside the STM scanner head. Which is located about 60cm below the cleaver.

Another essential part of the cleaving stage is radiation shielding. Radiation blocker in figure 3.1 b blocks room temperature radiation from the top part of the cryostat. Because it is made of thin Stainless steel of 0.4mm in thickness, it bends easily so that it bends

to make the path as the sample passes and recoils back to its original position. Push plate has a rectangular hole, which is perpendicular to the key hole, to prevent accidental passing through the cleaving stage without cleaving.

After sample is cleaved, one has to turn the sample transfer rod 90 degrees to go through the press plate. There are three of rectangular key holes normal to each other in the cryostat: 4K plate, cleaving stage and STM head. To pass each key hole, the sample stud must be rotated by 90 degrees. By means of these rotations, we can infer the location of the sample stud precisely and verify that sample stud is transferred correctly to the STM head.

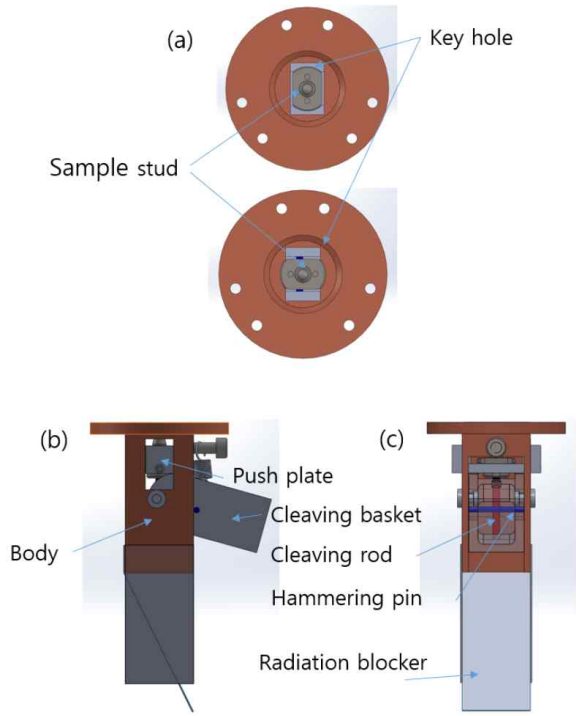

Figure 3.1 Schematic diagram of sample cleaving stage. (a) Top view of the sample cleaving stage. Key hole and sample stud are shown. By rotating sample stud, we can choose it to stay on top of the key hole (upper figure) or pass through the key hole (lower figure). (b, c) Side(b) and front(c) view of the sample cleaving stage. As sample stud presses press plate, press plate forces cleaving basket to rotate toward the body. Cleaving rod is attached to cleaving basket. Red rod is cleaving rod and blue rod is hammering pin.

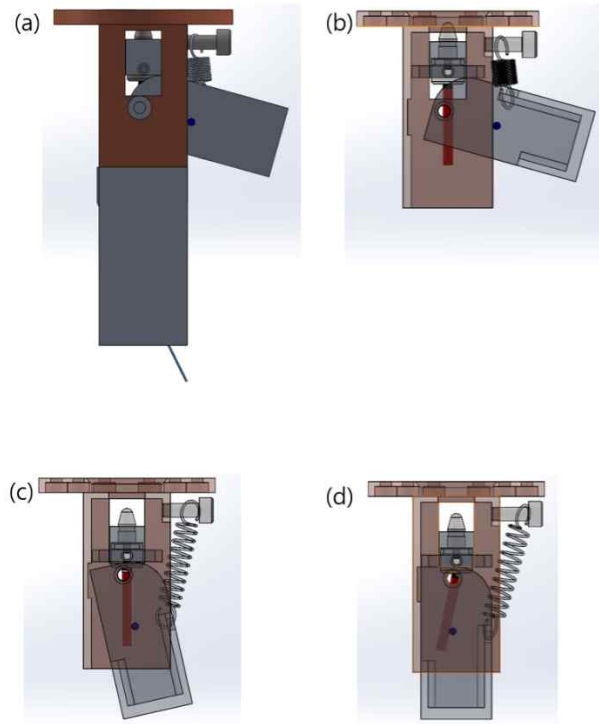

Figure 3.2 Procedure of sample cleaving. (a) Side view of cleaving system with sample stud, sample and cleaving rod. (b) Transmitting view before pressing press plate. (c) Transmitting view when hammering pin(blue) hits cleaving rod(red). (d) Transmitting view after cleaving.

3.2 Scanning Head

Head is the main part of measurement. It contains tip, sample, walker and rotator. Walker makes it possible that tip approaches to sample without damage. Rotator changes target of tip from gold to sample vice versa. Walker and rotator are operated by piezoelectric sheer stacks. Structure of head somewhat complex. It will be described below.

3.2.1 Piezo Motor for Walker

Walker is system which makes tip approaches to sample. The main part of walker is piezoelectric sheer stack. Piezo electricity is the phenomena of accumulation of electric charge in certain material in response to applied mechanical stress. Piezoelectric material is used to manipulate tip. With piezoelectric material, Tip approaches to sample or retracts from sample without significant heat or vibration. We use piezoelectric sheer stacks (PI, Inc.) for walker which is composed of 3 layers. It has 5 x 5 x 2.7 mm in volume and moves 1.5um/250V at room temperature. There are several methods of 'walks'. One is slip-stick motion.

Slip-stick method is illustrated in figure 3.3. It has become popular in low temperature instrument. Actually, we use 6 sheer piezoelectric stacks for walker; only 4 stacks are illustrated in figure 3.3. A single step consists of sequential sliding motion and a carrying motion. In the sequential-sliding action, each of the six stacks consecutively slides backward along the surfaces of the moving part. Because of the friction forces at the remaining five stacks, the moving part remains stationary while each stacks slides backward. In the carrying motion, all six stacks simultaneously return to their

original position and carry the moving part forward one step. Voltage versus time graph illustrated in figure 3.3. Another method is sliding motion. Unlike slip stick method, it is worked by single bias voltage.

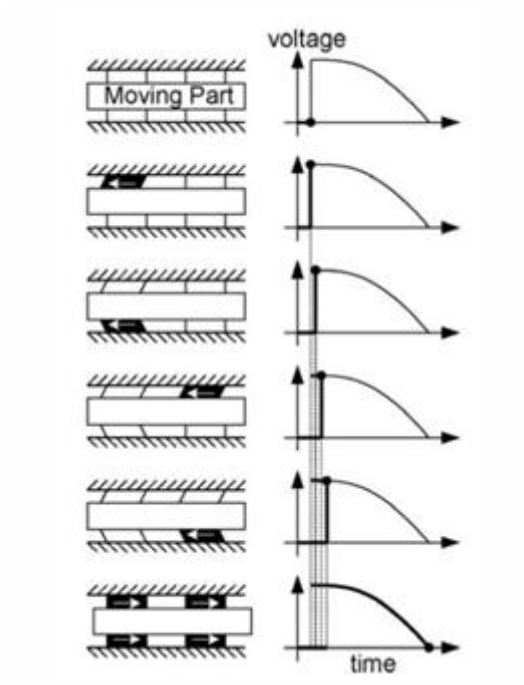

Figure 3.3 Slip-stick motion. Common approach for using small displacement of piezoelectric actuator to achieve long travel range. Walking motion method[11].

Operating voltage waveform is sawtooth waveform. By this voltage, sapphire prism is moved with a sliding motion. That is shown at figure 3.4. Unlike slip-stick motion, all piezo sheer stacks move together. When bias voltage increases gradually, piezo sheer stacks move sapphire prism. After increase of bias voltage, the voltage is droped rapidly. It makes piezo sheer stacks move backward

rapidly. By inertia of sapphire prism, piezo stacks can move backward while the prism doesn't move. Tough figure 3.4 represents 500Hz waveform, we can manipulate rotator at various voltage and various frequency. PMD4 of nanonis generates waveform like figure 3.4. By this voltage, walker can walk to sample. Figure 3.5 shows a diagram of the piezoelectric motor used in the STM, head of STM. 'Walk' is done with feedback circuit. Before walk, tube scanner made of piezoelectric material sweeps the space to check the tip reaches set point or not. If tip doesn't reach the set point, walker walks one step. After walk, piezoelectric motor repeat these procedures until tip reaches set point.

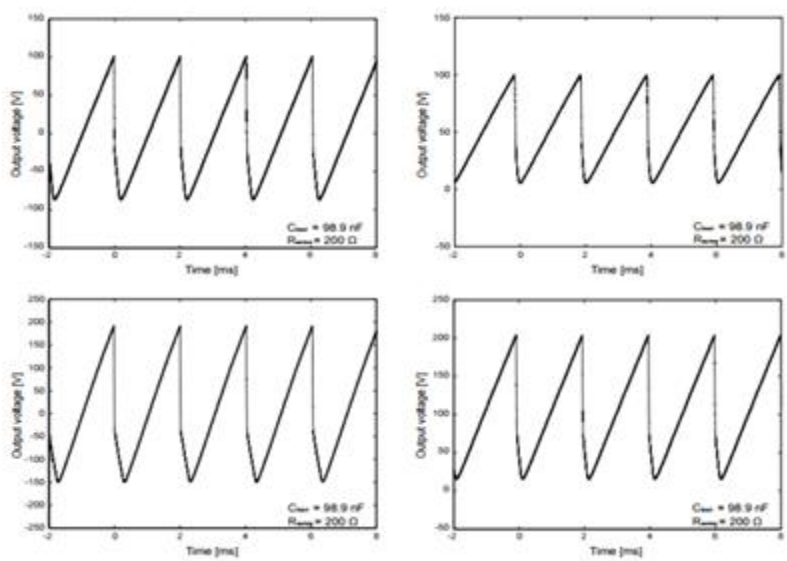

Figure 3.4 Output waveforms of piezo control driver at 500Hz. The left column shows bipolar waveforms and the right column shows unipolar waveforms.[12]

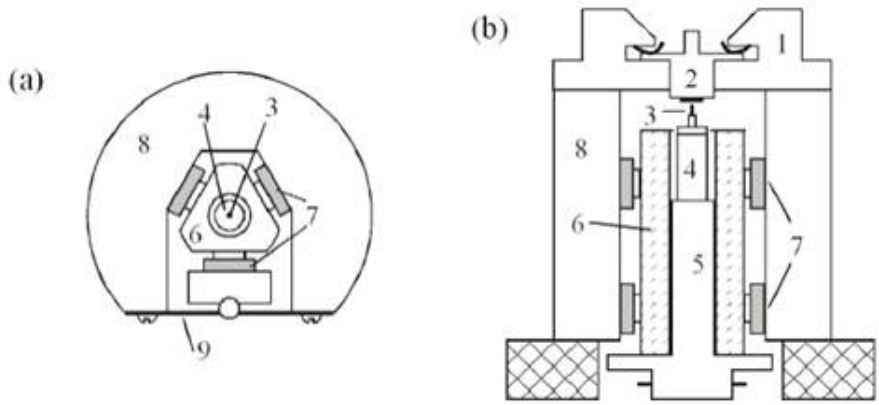

Figure 3.5 The STM head with piezo motor. (a) top view and (b) side view. (1) Sample Receptacle, (2) Sample Holder, (3) Tip, (4) Tube Scanner, (5) Scanner Holder, (6) Sapphire Prism, (7) Shear Piezo Stacks, (8) Macor Body, (9) Spring Plate (not to scale).[13]

3.2.2 Field Emission Stage (Rotator)

Field emission technique is widely used for STM tip treatment. By applying high voltages (100~300V) on gold target, high field emission current, at most order of microampere, flows between gold-tip junction. While this happens, tip apex becomes sharper at the same time oxide layer presented on the tip can be removed. Field emission technique is one of the most powerful tip treatment method can be performed *in-situ*.

In order to perform field emission technique, we used two methods for changing sample to gold target. First method is that simply taking out sample and transfer gold target. This method is simple, however, we need to discard the sample and it consumes at least 24 hours. Not to discard sample, we attach sample and gold target on the same sample stud but with small offset from the center of the sample stud. By tilting the STM tip slightly and rotating the sample stud, we can choose which target to approach. This method allows us to save the sample as well as time, however, it still consumes many hours and more importantly, tilting angle of tip and sample preparation must be very precise to approach both samples. Moreover, because of this alignment, the size of sample must be somewhat bigger.

In-situ field emission stage enables tip treatment without exchanging or removing the sample. Since we don't need to change or rotate the sample stud, tip treatment time requires only about 3~4 hours including approaching gold target and re-approaching sample, but excluding field emission time. In addition, we don't need to break vacuum. Overall, we can maintain non-invasive measuring environment. Moreover, we can utilize this stage as multi-purpose sample stage by replacing gold target to other samples or attaching

them both.

We designed the field emission stage which has an ability to rotate gold sample on and off of the tip. Figure 3.6 shows the field emission stage. Gold sample is on the sapphire plate (custom, from Lstone company) and two pairs of the piezoelectric shear stacks (P111.0X from Physik Instrument L. P.) are located above and below the sapphire plate. Bottom two piezoelectric shear stacks are glued with epoxy on STM head body and top two piezoelectric shear stacks are glued with epoxy on BeCu plate (figure 3.6 c). Ruby balls are held in the contraption on the BeCu plate and press the BeCu plate by springs on top of the ruby balls. Bolts on top press springs and control the tension of the springs. We can adjust the step size of the piezo stacks by tightening/loosening the bolts. Such with the slip-stick motion of the piezoelectric shear stacks, as the piezoelectric stacks elongate (shrink) in the circumferential direction, these linear motion makes the sapphire plate to rotate counter-clockwise (clockwise) and the total rotation angle is 35 degrees. The operating voltage has sawtooth waveform with variable voltage amplitude and frequency.

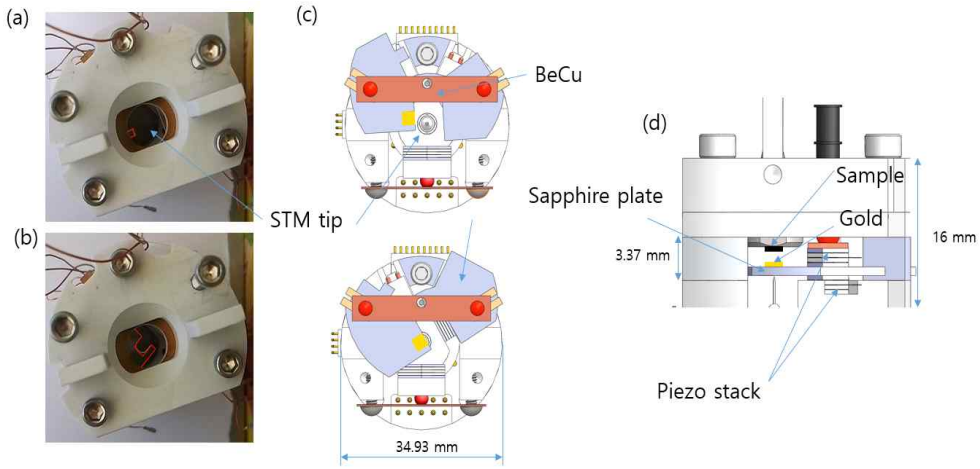

Figure 3.6 Top view and side view of rotator. Top view of STM head. When gold is (a) out of tip position and (b) on tip position. Red lines reveal the sapphire plate of rotator. (c) Top view of STM head with removing top parts for more clearance. (d) Side view of STM head. There are 2 sets of PZT top and bottom of the sapphire plate. Bottom pzts are attached to STM head body and top pzts are pressed by BeCu pressure plate, ruby balls. Linear motion of PZTs are converted to rotation. Volume of sample and gold is overestimated to see.

We can record the position of the sapphire plate by measuring capacitance between tip and gold. Capacitance is measured by capacitance bridge (Model AH2550A from Andeen-Hageling). Steps versus capacitance curve at 160V, 200V and 240V at 4.2K is shown at figure 3.7 (b). Each plots are measured at 4.2K temperature and the capacitance is measured between tip and gold. Capacitance is measured at each 20000 steps. When the gold is on the tip position, capacitance is 0.079pF and when the gold is out of tip position,

capacitance is 0.0248pF. To rotate gold on (out of) the tip position, it needs 40,000 steps at 180V and room temperature and 280,000 steps at 240V and 4.2 K.

Caution is needed in the operation of FE stage. Due to the fact that number of the steps required for the full range rotation of the sapphire plate is great and also operation voltage is as high as over 200V, a continuous stepping of the piezo sheer stacks can result in an abrupt increase of the head temperature. Appropriate number of steps at a time without sudden temperature rise was less than 50k steps at about 1 kHz.

Due to the miniature size of our STM head assembly, there are several limitations to design this stage. Gold and sample must not be in touch, and yet their distance must be minimized because of the tip traveling distance as short as 4mm. To shorten tip traveling distance, we needed to adopt use smaller piezo sheer stacks (3.5x3.5x2.2mm, two sheer plates) than the ones used for the piezo walker motors (5x5x2.7mm, three sheer plates) for the scanner.

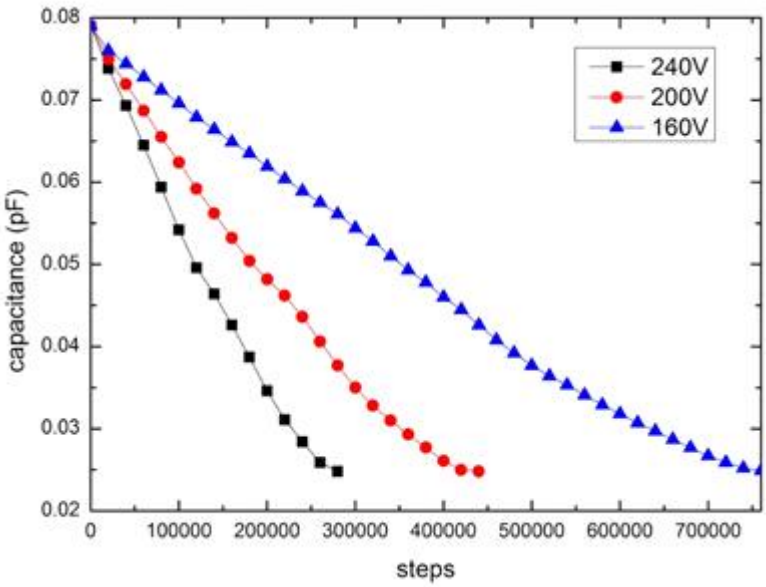

Figure 3.7 Performance of rotator at different voltages at 4.2K. Capacitance versus steps for 240V, 200V and 160V. Gold-in state is 0.79pF in capacitance and gold-out state is 0.248pF in capacitance.

3.3. Laboratory Design for Vibration Isolation

Because the tunneling current is exponentially sensitive to the tip-sample distance, the ability to suppress vibration and acoustic noise is essential for high quality data acquisition in tip-sample junction. For the efficient use of space, the goal of the laboratory design is achieving the most compact design with a maximized vibration isolation ability. Description of our laboratory is described in figure 3.8.

We dug a pit hole below the floor level and made concrete base and concrete block over concrete base. To isolate vibration from the concrete base, 6 air springs (Model PD-1001H from Integrated Dynamics Engineering) were placed between concretes base and

block. All the conduits for pumps and gas insertions are in the concretes base and block. They are interconnected by bellows and connected to pumps in the separate room to isolate vibration and acoustic noise from the pumps.

The pit hole plays a crucial role in maintenance. There is ladder which allow to go down to ground floor and vacancies which are enough to enter 180cm tall person to manipulate bellows which connect pumps room and experiment room. Existing design requires extra space for maintenance but with our pit hole design, we can save the space by half of the existing design. The hole is covered by soundproof materials to isolate the acoustic noise while we operate experiments.

Concrete block is made of high-density concrete to increase inertia mass. The density of the concrete block is 3350kg/m^3 and the total weight is about 30 tons. Its density is 1.4 times denser than that of normal concrete block of 2400kg/m^3. It is made of mixture of normal concrete and ironstone to increase its density.

Acoustic room is on the concrete block and STM is installed in the acoustic room. Plate for STM is placed on top of the three air springs on the legs (from Technical Manufacturing Corporation). The legs and plate are filled with lead shots to increase inertia mass. STM cryostat and dewar are only attached to STM plate. When we need to work on STM head and cryostat, we lower the dewar in the pit hole through the hole in the concrete block. In order to move heavy equipment inside the acoustic room, there are two hooks on the ceiling for adopting ceiling hoist. Due to the limited laboratory space, it is difficult to put heavy lifting equipment inside the room. Ceiling hoist can be hung on the ceiling hooks so that we can move heavy equipment easily. Since these hooks are installed on the

building ceiling, not on the acoustic room ceiling, it can hold heavier weight at the same time we can save the space further. In addition, by designing the hooks not to protrude the acoustic room ceiling, we can conceal them by closing hatches on the acoustic room ceiling and isolate acoustic noise from hook area.

PVC pipes for signal lines are buried in the concrete block. Signal lines are connected from STM to control room through the PVC pipes and margin of PVC pipes are filled with soundproof materials. Every experiments is controlled only in control room. Because of shortage of height, concrete block is lower than original floor and to overcome the height difference, there is false floor which is also useful to access the top of STM table.

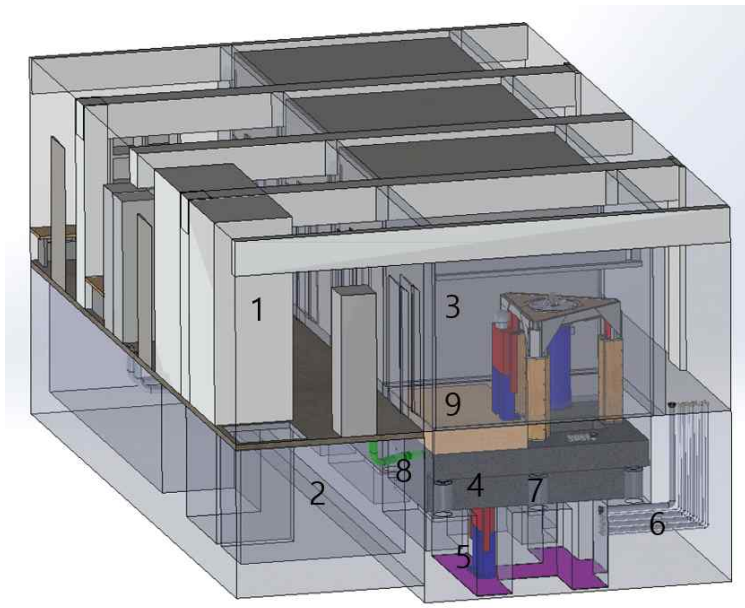

Figure 3.8 Schematic diagram of STM room. Researchers control experiment in the control room (1). Attaching sample to sample stud and cleaving rod to sample is performed in preparation room (2). Probe and Dewar are in the acoustic room (3) and on the concrete block (4). Concrete block is on the concrete foundation (5) and there are 6 air springs between them. Pump lines (6) are buried in concrete block and foundation. They are linked by bellows and connected to pumps in pump room (7). Signal lines are extended to control room by through signal line tubes (8) buried in concrete block and preparation room. To overcome low-level ceiling, dig up construction is performed. Because of the construction, control room and acoustic room have different floor level. To resolve that matter, false floor(9) is located.

Chapter 4
Performances of STM

4.1 BSCCO Data Aquisition

As we already mentioned, our STM design can sharpen tip without any manipulation from outside. *In-situ* tip sharpening gives high quality topographic image and spectroscopy data. Figure 4.1 displays images of two surfaces. Left image is field of view of gold after field emission and right image is field of view of BSCCO after field emission. Gold surface shows smooth topograph. The BSCCO plane clearly shows atoms. Upper image is 10nm square and lower image is 120nm square. The conditions are followed, I = 10pA , V = 100mV (left), V = 200mV (right), P-gain = 1nm, I-gain = 40nm/s and 1 time/line(s) (left), 17.88 time/line(s) (right). For BSCCO, total acquisition time is 42912sec. Along the red arrow, we can clearly see supermodulation.[13] BSCCO unit cell consists of combination of pyramid structure and NaCl structure. To lower the energy of structure, lattice constants are changed slightly. As a result of changes, structure of BSCCO reveals cosinusoidal variation. This is supermodulation and the effect is visible as corrugations of the BSCCO surface. Along the green arrow, we can see dollar signs. These are vacancies of bismuth atoms.

Our initial STM test was performed on the high-T_c superconductor overdoped BSCCO with T_c~60K at 4.2K. All data were taken with Nanonis SPM controller and Femto DLPCA 200 preamplifier with 10^9V/A gain and full bandwidth.

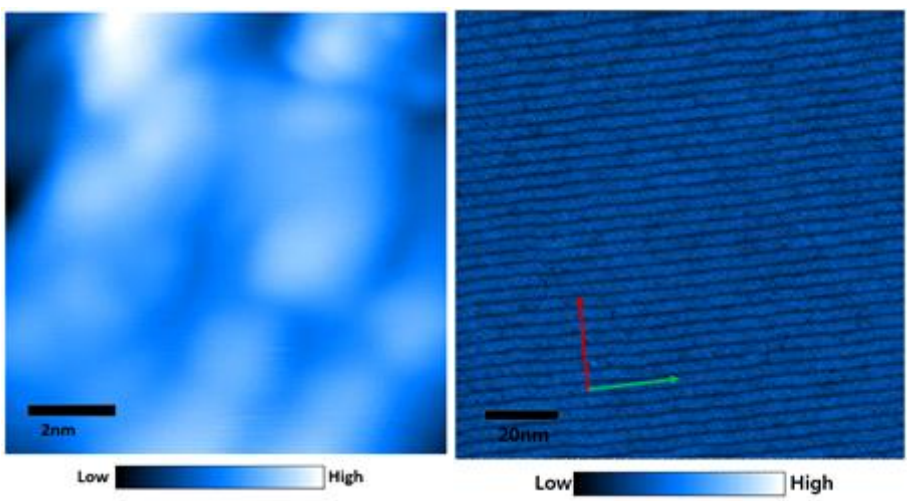

Figure 4.1 Result of tip sharpening. Topograph of Gold and BSCCO (Tc ~ 81K) surfaces. (Left) Topograph of gold after tip treatment by field emission. (Right) Topograph of BSCCO after tip treatment by field emission. Gold topograph (I_{set} = 10pA, V_{sample} = 100mV) shows smooth surface and BSCCO topograph (I_{set} = 10pA, V_{sample} = 200mV) shows clear atomic resolution. Left image is 10nm square size and right image is 120nm square size. Along the red arrow, we can see supermodulation. Along the green arrow we can see atomic vacancies.

The sample is transferred to the sample cleaving stage which is placed at the 4K stage of cryostat. Before sample cleavage, the sample stay there an hour, then cleaved. After sample cleavage, sample is immediately transferred to the STM head. It is critical to

transfer the sample rapidly to keep the clean sample surface.

After the sample transfer, by rotating gold target to the tip position, tip-gold junction is formed. Tungsten tip is cleaned by using field emission technique. Measuring topograph, $I-V$ characteristics and dI/dV spectrum verify the good tip condition. When tip is ready to measure high-resolution imaging, rotate the gold target out of the tip position and tip is approached to the sample.

In Figure 4.2 shows the measured data. All data were taken simultaneously in the same field of view (FOV) with size of 500x230 Å/255x118 pixels. It takes about 18 hours to measure the data and no filters are applied on the data shown here. Figure 4.2.a shows measured topograph (constant current mode, I = 100pA, V_{sample} = 100mV). Supermodulation features and atomic corrugation are clearly observed. It verifies that we achieve a high-resolution tip. At the same time, differential conductance map at V_{sample} = 22mV in Figure 4.2.b shows successful high-resolution spectroscopy. The junction resistance was 1GOhm and we used a lock-in technique to measure the dI/dV spectra. We used 2mV_{rms} modulation bias voltage with 1.3kHz modulation frequency. Line profile (Figure 4.2.c) along the red line in Figure 4.2.b shows coherence peaks and V-shaped spectrum inside the gap. Meanwhile, from Figure 4.2.b, we can obtain the spatial gap distribution of the gap as in Figure 4.2.d. The histogram of all gap values in the entire FOV is presented in Figure 4.2.e. The averaged gap value is 13.65mV. This is well matched the fact that the sample is quite highly overdoped BSCCO.

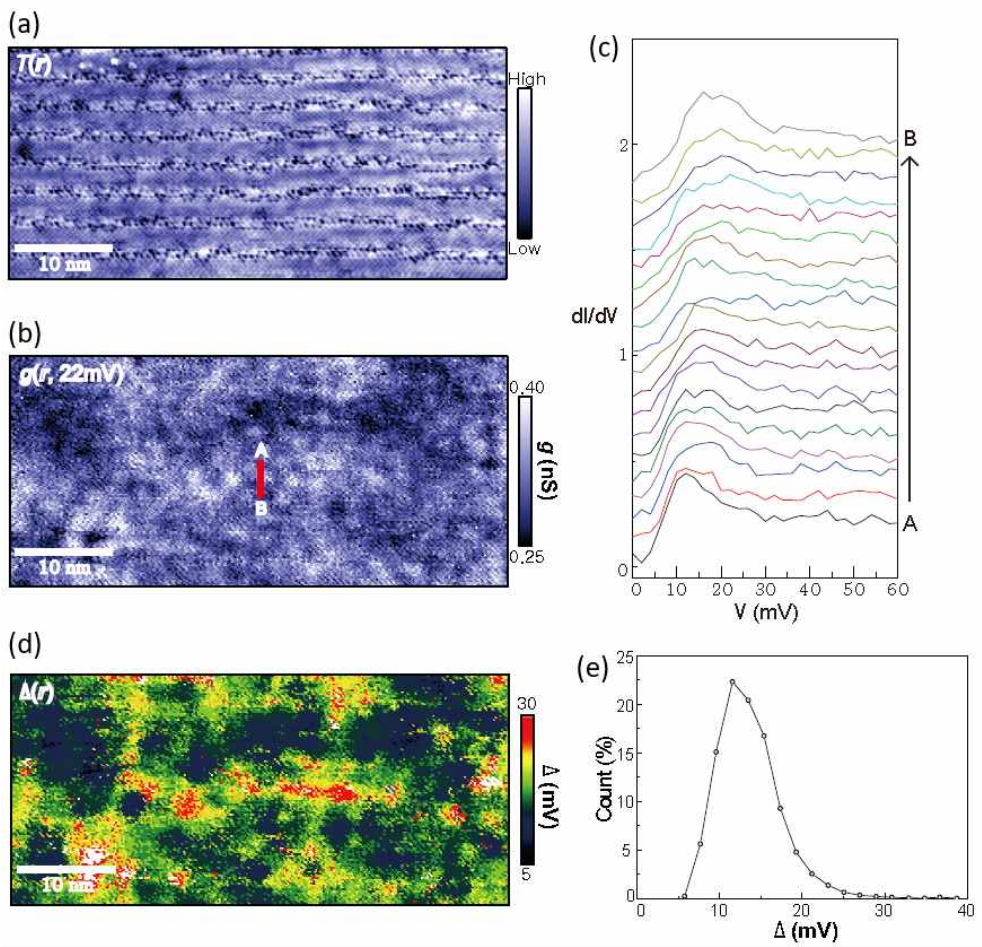

Figure 4.2 Overdoped BSCCO data. Measured data on Bi2Sr2CaCu2O8+x at 4.2K. All data here were taken simultaneously in the same field of view with size of 500x230 Å/255x118 pixels. (a) Topograph (constant current mode, I = 100pA, V_{sample} = 100mV) image shows clear supermodulation features and atomic corrugation. (b) Differential conductance map measured in the same FOV in (a). The junction resistance was 1GOhm. Here, we used a lock-in technique with fmod=1.3kHz and Vmod=2mV$_{rms}$. (c) Line profile along the red line in (b). Vertical offset is imposed for clarity. Coherence peaks and V-shaped spectrum inside the gap are clearly visible. (d)

Gapmap shows spatial distribution of the gap. The averaged gap value is 13.65 mV. (e) A histogram of all gap values in the field of view shown in (c). The peak is located at 13.48mV.

4.2 Scanning Josephson Tunneling Microscopy

Another application of our LT-STM is scanning Josephson tunneling microsopy (SJTM). Recently, M. H. Hamidian *et al.*[15] reported successful SJTM experiment at 50mK. SJTM experiment at 4K, however, has not been reported yet.[16,17] Here, we present SJTM result at 4.2K.

Prerequisite of the SJTM experiment is superconducting tip. To obtain superconducting tip, a tungsten tip approaches to BSCCO sample in a very close distance so that a nanometer-sized flake of BSCCO is attached to the tungsten tip. In this way, we can obatain BSCCO-tip. By manipulating the tip-sample distance, we can form single particle-tunneling regime SIS (superconductor Insulator superconductor) junction and pair-tunneling regime Josephson junction between BSCCO-tip and BSCCO sample.

We have used the same overdoped BSCCO sample as in section 4.1. Figure 4.3 shows the measured data from BSCCO-tip. Figure 4.3 a-c displays the simulataneously measured single particle-tunneling SIS junction data. The field of view has size of 600x265 Å/255x133 pixels. Atomic corrugation and supermodulation features are clearly visible, although atomic vacancies are not observed. Since the tip apex cannot have a single atom radius, the SIS topograph is a convoluted image of two BSCCO topograph. However, the fact that we can resolve the atomic corrugation proves our BSCCO-tip has a high-resolution ability. Figure 4.3 b demonstrates the SIS differential conductance map at V_{sample} =

-38mV. Figure 4.3c is dI/dV spectrum extracted from the Figure 4.3 b. Since the tip has changed to superconductor from normal metal, the coherence peaks of SIS dI/dV spectrum (black solid curve) occur at 34 mV meanwhile the SIN (superconductor-insulator-normal metal) junction dI/dV spectrum (red dashed curve) shows the coherence peaks at 14 mV. This proves our tip certainly has became BSCCO-tip with Δ_{tip} = 20 mV. Figure 4.3 d&e show the STJM experiment results. As the tip approaches the sample close enough to form the Josephson junction, we observe the zero bias conductance peak (ZBCP), which indicates the existence of the Josephson supercurrent, as in figure 4.3 e. ZBCPs are observed in the entire field of view of the current map (256x256 Å/128x128 pixels/3 MOhm junction) (figure 4.3 d) and this demonstrates that we successfully measure the Josephson supercurrent map.

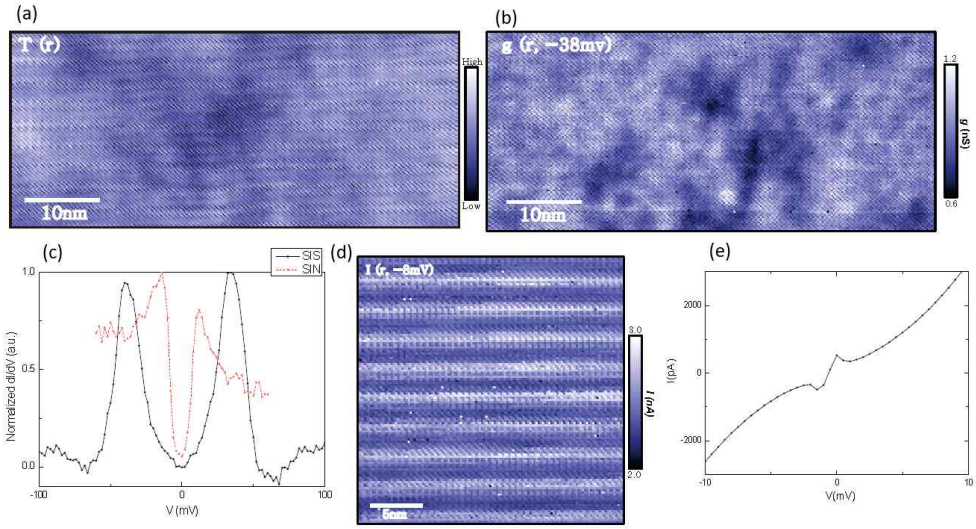

Figure 4.3 SJTM on Overdoped BSCCO. Measured data on $Bi_2Sr_2CaCu_2O_{8+x}$O by using BSCCO-tip at 4.2K. (a) Topograph (I_{set} = 10 pA, V_{sample} = 100 mV) in single particle-tunneling regime SIS junction. Size of the topograph is 600x265 Å/255x133 pixels. Supermodulation feature and atomic corrugation are visible although atomic vacancies are disappeared. (b) Differential conductance map at Vsample = -38 mV (1GOhm junction) in single particle-tunneling regime. (c) dI/dV spectrum extracted from (b) is shown in black solid curve. Red dashed curve shows dI/dV spectrum of SIN junction. The location of the coherence peaks are shifted by 20 mV from 14 mV (SIN junction) to 34 mV (SIS junction). This indicates that our tip becomes BSCCO-tip with Δtip = 20 mV. (d&e) By approaching the BSCCO-tip very close to the sample, we can form the Josephson junction between tip and sample. Current map (3 MOhm junction/256x256 Å/128x128 pixels) (d) and $I-V$ characteristic (e) demonstrate SJTM experiment result. Zero bias conductance peak in (e) which indicates the existence of the Josephson supercurrent occurs in the entire field of view of the current map (d).

Chapter 5
Conclusions

5.1 Summary

In this thesis, STM systems for vibration isolation and tip and sample preparing system were investigated. Also, Labview programming for experiment control and C programming for data conversion were introduced. Specifically, sample cleaving system makes it possible that sample preparation can be done without oxidation. Remote controllability and high vacuum circumstance give high quality sample suface.

Tip treatment system (Rotator) makes *In-situ* field emission possible, which enables tip treatment without exchanging or removing the sample or tip. *In situ* tip preparation shorten data acquisition time and reduces risk of damage. Without vibration isolation, these tip and sample preparation systems have no use. High density concrete block and 9 air springs give high level of vibration isolation. With these preparation systems and vibration isolation system, we could acquire atomic resolution and scanning tunneling spectroscopy maps.

Micro-customization was done by Nanonis programming interface. It makes it possible that perform ungiven experiments like ‘change setpoint bias spectroscopy’ and ‘use external lock-in

spectroscopy'. The problem of data analysis program was solved by converting data format. Though there are some data lose, the solution for this problem was introduced. With all these efforts, we could get high quality data and we had ability to manipulate data.

5.2 Future Works

As I mentioned before, data conversion from float to unsigned short must loses accuracy. Change data format of 1FL file to float is fundamental solution. But, the complexity of structure of WAutility makes it difficult. Easy solution to improve data accuracy is removal of bad data before conversion. Unlike 3DS format, 1FL has only 65535steps resolution. Irregularly large points make data range longer. As result, data resolution (data range/65535) increase. By remove those point at 3DS data, we can get higher resolution than bad peak removed data from 1FL.

Bibliography

1. G. Binnig, H. Rohrer, *Scanning tunneling microscopy.* Helvetica Physicca Acta, 55, 726-735, 1982.

2. G. Binnig, H. Rohrer, C. Gerber, and E. Weibel. , *Tunneling Through a controllable vacuum gap.* Appl. Phys. Lett. , 40, 178, 1982.

3. G. Binnig, H. Rohrer, C. Gerber, and E. Weibel. , *Surface Studies by Scanning Tunneling Microscopy.* Phys. Rev. Lett. , 49, 57, 1982.

4. S. Misra et al. , *Design and performance of an ultra-high vacuum scanning uenneling microscope operating at dilution refrigerator temperatures and high magnetic fields.* Rev. Sci. Instrum, 84, 103903, 2013.

5. H. Kambara, T. Matsui, Y.Niimi, and H. Fukuyama. , *Construction of a versatile ultralow temperature scanning tunneling microscope.* Rev. Sci. Instrum, 78, 073703, 2007.

6. M. Assig, M. Etzkorn, A. Enders, W. Stiepany, C. R. Ast and K. Kern. , *A 10mK scanning tunneling microscope operating in ultra high vacuum and high magnetic fields.* Rev. Sci. Instrum. , 84, 033903,

2013.

7. Jinho Lee, K. Fujita, K. McElroy, J. A. Slezak, M. Wang, Y. Aiura, H. Bando, M. Ishikado, T. Masui, J.-X. Zhu, A. V. Balatsky, H. Eisaki, S. Uchida, and J. C. Davis. *Interplay of Electron-Lattice Interactions and Superconductivity in* $Bi_2Sr_2CaCu_2O_{8+\delta}$, Nature. , 442, 546-550, 2006.

8. K. Fujita, A. R. Schmidt, E.-A. Kim, M. J. Lawler, D.-H. Lee, J. C. Davis, H. Eisaki, S. Uchida. *Spectroscopic Imaging Scanning Tunneling Microscopy Studies of Electronic Structure in the Superconducting and Pseudogap Phases of Cuprate High-Tc Superconductors*, J. Phys. Soc. Jpn. , 81, 011005, 2011.

9. C. Julian Chen , *OIntroduction to scanning tunneling microscopy.* Oxford University Press , 2nd, 56p , 1989

10. SPECS. *Nanonis SPM Control software Documentation*, 06 2012.

11. King-Fu Hii, R.Ryan Vallance, M pinar Menguc. *Design, operation, and motion charateristics of a precise piezo-electric linear motor.* Precision Engineering 34:231 - 241, 2010.

12. SPECS. *Piezo Motor Driver PMD4 User Manual*, May 2013.

13. E. Hudson. *Investigating High-Tc Superconductivity on the Atomic scale by Scanning Tunneling Microscopy*. PhD thesis, UNIVERSITY OF CALIFORNIA AT BERKELEY, 1999.

14. J. A. Slezak, Jinho Lee, M. Wang, K. McElroy, K. Fujita, B. M. Anderson, P. J. Hirschfeld, H. Eisaki, S. Uchida, J. C. Davis , *Imaging the impact on cuprate superconductivity of varying the interatomic distances within individual crystal unit cells.* PNAS, 105, 3203-3208, 2008.

15. M. H. Hamidian, S. D. Edkins, Sang Hyun Joo, A. Kostin, H. Eisaki, S. Uchida, M. J. Lawler, E. -A. Kim, A. P. MacKenzie, K. Fujita, Jinho Lee, J. C. Séamus Davis , *Detection of a Cooper Pair Density Wave in* $Bi_2Sr_2CaCu_2O_{8+x}$. Nature, 532, 343, 2016.

16. Naaman, O., Teizer, W. & Dynes, R. C. , *Fluctuation dominated Josephson tunneling with a scanning tunneling microscope.* Phys. Rev. Lett. , 87 , 097004, 2001

17. Rodrigo, J. G., Suderow, H. & Vieira, S , *On the use of STM superconducting tips at very low temperatures.* Eur. Phys. J. B. , 40 , 483-488, 2004

APPENDIX

Labview code for Spectroscopy Experiment

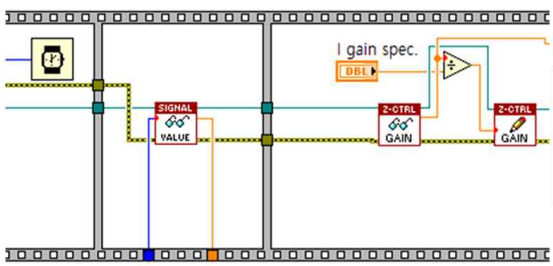

Lower the speed of tip movement

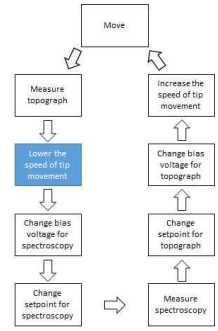

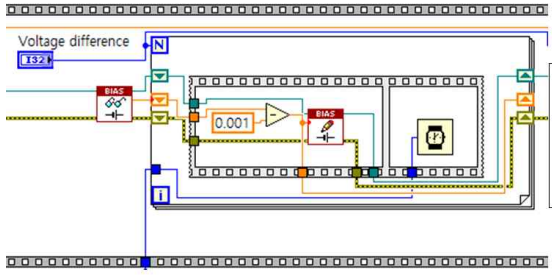

Change bias voltage for spectroscopy

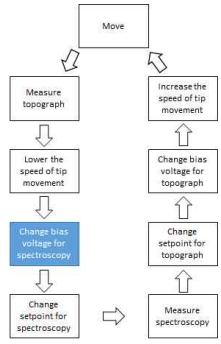

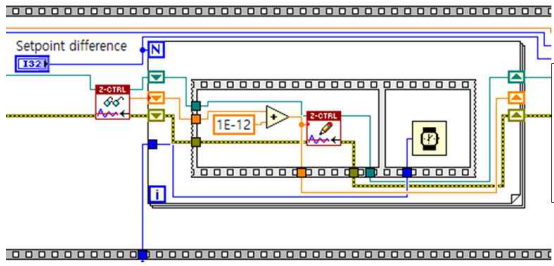

Change setpoint for spectroscopy

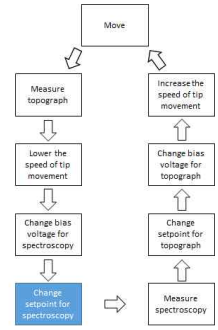

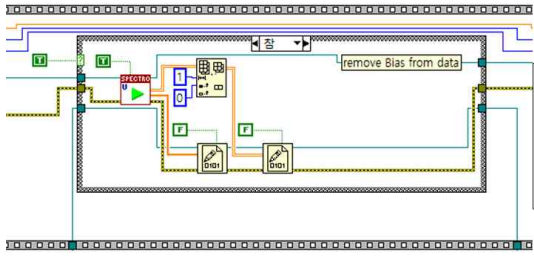

Measure Spectroscopy

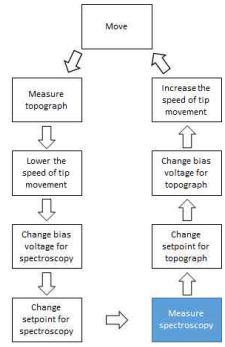

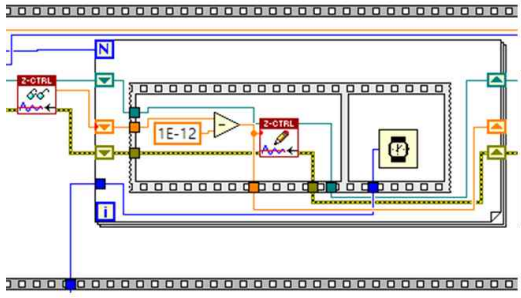

Change setpoint for topograph

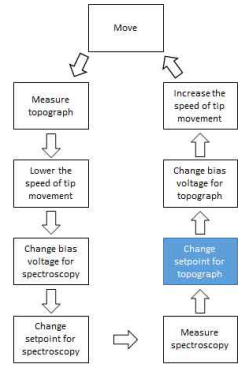

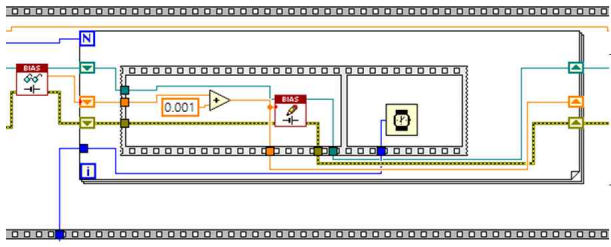

Change bias voltage for topograph

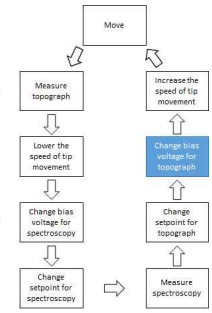

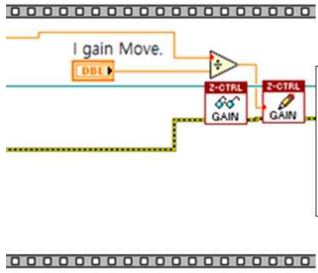

Increase the speed of tip movement

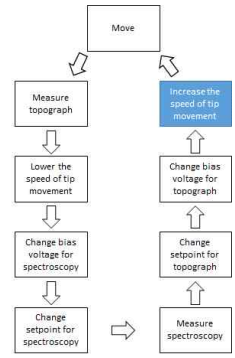

Data Conversion

```
#include<stdio.h>
#include<stdlib.h>
#include<string.h>
#include<stddef.h>
#include<stdlib.h>
#include<math.h>
#include<iostream>

typedef short BOOL16;
#define PI 3.141592653589793
float Varread(FILE *p){
        char a[5] = { 0, }, b[5] = { 0, };
        float c =0 ;
        fread(&a, 1,sizeof(char)*4, p);
```

```
        b[0] = a[3];
        b[1] = a[2];
        b[2] = a[1];
        b[3] = a[0];
        memcpy(&c, b, 4);
        return c;
}
void findequal(FILE *p){
        int i;
        char dumone[1];
        for(;;){
        fread(dumone, sizeof(char), 1, p);
        if (dumone[0] == '=')
        break;
        }
}
float distance(float a, float b, float c, float d){
        float e;
        e = (a-b)*(a-b) + (c-d)*(c-d);
        e = sqrtf(e);
        return e;
}
float rounding(float a){
        float b;
        b = floor(a+0.5);
        return b;
}
// Get conductance from rawdata
unsigned short dataconversion(float max, float min, float data){
        return (unsigned short) 65535*(data-min)/(max-min);
}
void main(void)
{
        int i, j, k, format;
        int gridX, gridY;
        int Ipoint;
        int day, month, year, hour, min, sec;
        int calint;
        float calfloat, rangeX, rangeY, Xmax, Ymax;
        float gridstartX, gridstartY, gridendX, gridendY, gridangle;
        float biasstart, biasend, X[256][256], Y[256][256], Z[256][256], Zoffset, settime, inttime,
```

```
FinZ, Zonoffget, unknown;
        float maxLIX, minLIX, avrLIX, stdLIX;
        char onedum[1], dummy[2048];
        unsigned short d;

        FILE *file, *fw, *fref;
        file = fopen("161102.3ds", "rb");//read 3ds file
        fw = fopen("161102.1FL", "wb");// write 1fl file
        fref = fopen("80810272.1FL", "rb");//reference file//
        //ftest = fopen("test.txt", "w");

        //read reference file//
        char szRelease[12], space0[2], szDate[16], space3[2], szTime[16], szDescription[40],
Filler0[184], space1[4];
        char szWorldUnit[10], szXYUnit[10], szRateUnit[10], szXUnit[10], cFiller[424],
cFiller1[142], cFiller2[370];
        float fPosX[8], fPosY[8], fXmin, fXmax, fYmin, fYmax, fDACtoWorld,
fDACtoWorldZero;
        short iCurves, iWorldUnitType, iXYUnitType, iLayers, bHasEchem, bHasBkStrip,
iPts[8], iXUnitType;
        short iTilt, iScaleZ, iFilter, iShading;
        short rRoix1, rRoix2, rRoiy1, rRoiy2;
        double dTiltC[8];
        int iRows, iCols;
        long iRelease, iOffset;
        unsigned short iDACmax, iDACmin, iDACtoColor, iDACtoColorZero,
iDACDisplayRange, iDACDisplayZero;
        BOOL16 bHasAcqDisplay;
        short iDataType, iDataDir, iDataMode, iCalibType, iLaserIntensity, iGain, iGainZ,
iReserve, iFilters, iHarmonic, iExpand;
        short iProbeType, iStageType, iCalFileSource, iSetpointUnits, iGainXY,
iCantileverType, iZlinearizer, bNonContact, CantileverType, iNonContactMode, iNonContactPhase;
        short bFeedbkPoints, bFeedbkCurves, bVzRelative, iExtLayer, bSpecialNCScan,
iRolloff, iXPosition, iYPosition, iOldGainXY;
        float fScanZmax, fScanZmin, fScanXmax, fScanYmax, fVtip, fI, fVz, fRange, fRate;
        float fPro, fInteg, fDer, fRotation, fModLevel, fAveraging, fSpCalFactor, fOverscanX,
fOverscanY, fNcRegAmp;
        float fHysteresisX[4], fHysteresisY[4], fHysteresisZ[4], fCrossTalkCoef,
fSensorResponse, fKc, fDriveAmplitude, fDriveFrequency;
        float fVzStart, fVzStop, fVzLimit, *fVzArray, fVzSpeed1, fVzSpeed2, fVzSpeed3,
```

```
fVzSpeed4, fVzPullback, iHalfCycles, iAvgPoint, fDelayStart, fDelaySample, fDelayPullback,
fDelayEstFeedbk;
        float fModFreq, fVzMod, fFrequency, fAmplitude, fPhase, fSensitivity, fTimeConst,
fOffset;
        unsigned short iScaleFactorZ, iDACminX, iDACmaxX, iDACminY, iDACmaxY,
iOffsetX, iOffsetY, iOffsetZ;
        unsigned short iOldOffsetX, iOldOffsetY, iOldDACminX, iOldDACmaxX,
iOldDACminY, iOldDACmaxY;
        char cScanType[6], szScannerSerialNumber[16], szStageType[64], szStageName[64],
szStageText[64];
        int iADC;
        //Read reference//
        //Header of reference file consists of two classes.
        //Each class consists of Documents information and scan parameter.
        //Because reading variables is simple task, we omit reading variable preocedure.

        //read 3ds//
        fread(dummy, sizeof(char) * 10, 1, file);
        fscanf(file, "%d", &gridX);
        fread(dummy, sizeof(char) * 3, 1, file);
        fscanf(file, "%d", &gridY);
        findequal(file);
        fscanf(file, "%f", &gridstartX);
        fread(dummy, sizeof(char), 1, file);
        fscanf(file, "%f", &gridstartY);
        fread(dummy, sizeof(char), 1, file);
        fscanf(file, "%f", &gridendX);
        fread(dummy, sizeof(char), 1, file);
        fscanf(file, "%f", &gridendY);
        fread(dummy, sizeof(char), 1, file);
        fscanf(file, "%f", &gridangle);
        findequal(file);
        findequal(file);
        findequal(file);
        findequal(file);
        findequal(file);
        findequal(file);
        fscanf(file, "%d", &Ipoint);
        findequal(file);
        findequal(file);
```

```
findequal(file);
fread(dummy, sizeof(char), 1, file);
fscanf(file, "%d", &day);
fread(dummy, sizeof(char), 1, file);
fscanf(file, "%d", &month);
fread(dummy, sizeof(char), 3, file);
fscanf(file, "%d", &year);
fread(dummy, sizeof(char), 1, file);
fscanf(file, "%d", &hour);
fread(dummy, sizeof(char), 1, file);
fscanf(file, "%d", &min);
fread(dummy, sizeof(char), 1, file);
fscanf(file, "%d", &sec);
for (;;){

fread(onedum, sizeof(char), 1, file);
if (onedum[0] == '_'){
break;
}
}
fread(dummy, sizeof(char) * 6, 1, file);
float current[256][256][256], LIX[256][256][256], LIY[256][256][256];
for (i = 0; i < gridX; i++){
for (j = 0; j < gridY; j++){
biasstart = Varread(file);
biasend = Varread(file);
X[i][j] = Varread(file);
Y[i][j] = Varread(file);
Z[i][j] = Varread(file);
Zoffset = Varread(file);
settime = Varread(file);
inttime = Varread(file);
Zonoffget = Varread(file);
FinZ = Varread(file);
for (k = 0; k < Ipoint; k++){
current[i][j][k] = Varread(file);
}
for (k = 0; k < Ipoint; k++){
LIX[i][j][k] = Varread(file);
}
```

```
for (k = 0; k < Ipoint; k++){

LIY[i][j][k] = Varread(file);
}
}
}
//find Max, Min value of Lock-in X//
maxLIX = LIX[0][0][0];
minLIX = LIX[0][0][0];
for (i = 0; i < gridX; i++)
{
for (j = 0; j < gridY; j++)
{
for (k = 0; k < Ipoint; k++)
{
if (LIX[i][j][k] >= maxLIX){
maxLIX = LIX[i][j][k];
}
if (LIX[i][j][k] < minLIX){
minLIX = LIX[i][j][k];
}
}
}
}

//write DocumentINfo//
//Data sequence same with 1FL file format is written.
//Only some key values are listed below
iDACmax = dataconversion(10, -10.001, maxLIX);
fwrite(&iDACmax, 1, sizeof(unsigned short), fw);
iDACmin = dataconversion(10, -10.001, minLIX);
fwrite(&iDACmin, 1, sizeof(unsigned short), fw);
calfloat = distance(X[1][2], X[1][1], Y[1][2], Y[1][1]);
calfloat = rounding(pow(10., 10.)*calfloat*gridX);
rangeX = calfloat;
fwrite(&rangeX, 1, sizeof(float), fw);
fwrite(&fYmin, 1, sizeof(float), fw);
calfloat = distance(X[2][1], X[1][1], Y[2][1], Y[1][1]);
calfloat = rounding(pow(10., 10.)*calfloat*gridY);
rangeY = calfloat;
```

```
fwrite(&rangeY, 1, sizeof(float), fw);
fDACtoWorld = (maxLIX - minLIX) / 65535.;
fwrite(&fDACtoWorld, 1, sizeof(float), fw);
fDACtoWorldZero = minLIX;
fwrite(&fDACtoWorldZero, 1, sizeof(float), fw);
std::cout << "topograph setpoint in nA : ";
std::cin >> fI;
fwrite(&fI, 1, sizeof(float), fw);// topo setpoint in nA
std::cout << "initial setting time in sec : ";
std::cin >> fDelayStart;
fwrite(&fDelayStart, 1, sizeof(float),fw);
fDelaySample = settime * 1000000;
fwrite(&fDelaySample, 1, sizeof(float),fw);
std::cout << "milliseconds wait in Labview  : ";
std::cin >> fDelayPullback;
fDelayPullback = fDelayPullback * 1000;
fwrite(&fDelayPullback, 1, sizeof(float),fw);
std::cout << "end setting time in in sec  : ";
std::cin >> fDelayEstFeedbk;
fDelayEstFeedbk = fDelayEstFeedbk * 1000000;
std::cout << "Lock-in frequency(Hz)  : ";
std::cin >> fFrequency;
fwrite(&fFrequency, 1, sizeof(float), fw);
std::cout << "Lock-in amplitude(mV)  : ";
std::cin >> fAmplitude;
fwrite(&fAmplitude, 1, sizeof(float), fw);
std::cout << "Lock-in phase  : ";
std::cin >> fPhase;
fwrite(&fPhase, 1, sizeof(float), fw);
std::cout << "Lock-in Sensitivity(V)  : ";
std::cin >> fSensitivity;
fwrite(&fSensitivity, 1, sizeof(float), fw);
std::cout << "Lock-in time constant(S)  : ";
std::cin >> fTimeConst;
fwrite(&fTimeConst, 1, sizeof(float), fw);
std::cout << "Lock-in Roll off  " << std::endl;
std::cout << "1 : 6dB, 2: 12dB, 3: 18dB, 4:24dB  " << std::endl;
std::cout << "select number : ";
std::cin >> iRolloff;
fwrite(&iRolloff, 1, sizeof(short), fw);
std::cout << "Lock-in Reserve  " << std::endl;
```

```
        std::cout << "1 : HIGH RESERVE, 2: NORMAL, 3:LOW NOISE    " << std::endl;
        std::cout << "select number : ";
        std::cin >> iReserve;
        fwrite(&iReserve, 1, sizeof(short), fw);
        fwrite(&iFilters, 1, sizeof(short), fw);//check 23167
        std::cout << "Lock-in harmonic  : ";
        std::cin >> iHarmonic;
        fwrite(&iHarmonic, 1, sizeof(short), fw);
        //write data
        for (int n = 0; n<Ipoint; n++){
        for (int y = 0; y<gridY; y++)
        for (int x = 0; x<gridX; x++){
                d = dataconversion(maxLIX, minLIX, LIX[gridY - y - 1][x][n]);
        fwrite(&d, 1, sizeof(unsigned short), fw);
        }
        }
        fclose(file);
        fclose(fw);
        fclose(fref);
        //printf("%f\n", inttime);
}
```

Abstract in Korean

국문 초록

저온 주사 터널링 현미경은 표면 과학뿐 아니라 응집 물질 물리 분야에서 가치있는 도구이다. 우리는 기존 초저진동 저온 주사 터널링 현미경에서 3 가지 개선점을 보였다. (팁 처리 장치, 시료 준비 장치, 진동 제거 시스템). 개선된 팁 처리 장치는 우리로 하여금 시료의 변화 없이 내부적으로 필드 에미션을 가능하게 하였다. 또한, 개선된 시료 준비 장치는 간단한 미는 동작만으로 직접 보지 않고 저온 진공 환경에서 시료 처리를 가능하게 하였다. 우리의 새로운 진동 제거 시스템은 효율적인 공간 사용과 진동 제거 능력을 제공한다. 이러한 개선점들은 몇 일간 지속되는 스펙트로스코피 이미징 실험의 질을 향상 시켰으며 향상된 데이터를 제공 하였다. 한편, 나노니스사의 주사 터널링 현미경 조작 장치는 기본적으로 일련의 실험들을 제공하는데, 이 실험들은 Labview 기반으로 구성되어 있다. 우리는 우리의 선택에 따라 커스터마이징 된 실험 프로토콜을 추가하였다. 게다가, 토포메트릭스사의 수 십년간 축적되어온 분석 라이브러리가 방대하고 포과적이기 때문에, 우리는 C++를 사용하여 완전히 새로운 라이브러리를 제작할 필요 없이 나노니스사의 데이터 형식을 토포메트릭스사의 데이터 형식과 호환이 가능하게 만들었다. 마지막으로, 우리는 스펙트로스코픽 이미징 주사 터널링 현미경의 4K에서의 성능을 보여주기 위해, 높게 도핑된 비스코 샘플을 기존 저진동 실험실보다 소형의 저진동 실험 설비를 통해 보여주었다. 이 논문에서 나는 이런 주사 터널링 현미경 장치에서의 개선점을 기술하고 컨트롤과 데이터 분석을 위한 소프트웨어적 측면도 기술하였다.